Electronic Supplementary Information

Oligo(aniline) nanofilms: From molecular architecture to microstructure

Thomas G. Dane,[a] Philip T. Cresswell,[a] Georgia A. Pilkington,[a] Samuele Lilliu,[b] John E. Macdonald,[c] Stuart W. Prescott,[a] Oier Bikondoa,[d] Charl F. J. Faul*[a] and Wuge H. Briscoe*[a]

[a] School of Chemistry, University of Bristol, Cantock's Close, Bristol, BS8 1TS, UK.

[b] Nano-Optics and Optoelectronics Research Laboratory, Masdar Institute of Science and Technology, Abu Dhabi, UAE.

[c] School of Physics and Astronomy, Cardiff University, Queens Buildings, The Parade, Cardiff CF24 3AA, UK.

[d] XMaS, The UK-CRG Beamline at the ESRF, 6 Rue Jules Horowitz, B.P. 220, 38043 Grenoble CEDEX 9, France and Department of Physics, University of Warwick, Gibbet Hill Road, Coventry, CV4 7AL, UK.

* Authors to whom correspondence should be addressed. Email: charl.faul@bristol.ac.uk; wuge.briscoe@bristol.ac.uk

Table of Contents

S1 Data Analysis

Images recorded on a planar detector must be transformed into reciprocal space maps *i.e.* an intensity map as a function of the in-plane scattering vector (Q_{xy}) and the out-of-plane scattering vector (Q_z). Such transformations require three main processes, as follows.

1. *Determination of scattering angles*. When the detector is oriented perpendicular to the incident beam the scattering angles can be deduced using simple trigonometric relationships. When this is not the case, *i.e.* the detector is rotated about any of the three axes relative to the sample, the resulting image will be distorted and must be corrected.
2. *Reciprocal space conversion*. To obtain the reciprocal space map from the scattering angles, a 2D non-affine transformation must be performed to represent the 3D scattering vectors projected onto a 2D plane.
3. *Refraction correction*. Waves of X-ray radiation crossing an interface are subject to refraction effects, resulting in a slight inaccuracy of the calculated Q_z values, which must be corrected for.

The equations used for each of these steps, and an explanation of the practical implementation of these transformations are documented in Sections S1.2 to S1.6 in this ESI. Additionally, the distance from the sample to the detector must be calibrated, as described in Section S1.1.

Table S1 List of important symbols used in the equations.

Symbol	Meaning
x, y, z	Lab frame coordinate axes
x', y'	Image frame coordinate axes
L_{SD}	Sample-to-detector distance
$2\theta_v$, $2\theta_h$	Vertical and horizontal detector angles
x'_{pix}, y'_{pix}	Image x and y pixel coordinates
x'_{dir}, y'_{dir}	Image x and y pixel coordinates of the direct beam
x'_N, y'_N	Image x and y pixel coordinates of the point of normal incidence
λ	X-ray wavelength
k	Wavevector
n	Complex index of refraction
δ, β	Scattering and absorption coefficients
k_i, k_f	Incident and reflected wavevectors
α_c	Critical angle
α_i, α'_i	Vacuum incident angle and film incident angle
α_{f0}, $2\theta_{f0}$	Out-of-plane and in-plane scattering angles (lab frame)
α_f, $2\theta_f$	Out-of-plane and in-plane scattering angles (surface frame)
Q	Absolute wavevector transfer
Q_x, Q_y, Q_z	x, y and z components of Q
Q_{xy}	In-plane component of Q

S1.1 Calibration of sample-to-detector distance

To accurately determine the reciprocal space coordinates of image pixels, the distance between the sample and the detector (L_{SD}) must be calibrated. This was performed by rotating the detector about the lab frame z- and y-axes and recording an image as shown in Fig. S1 (for rotation about the z-axis).

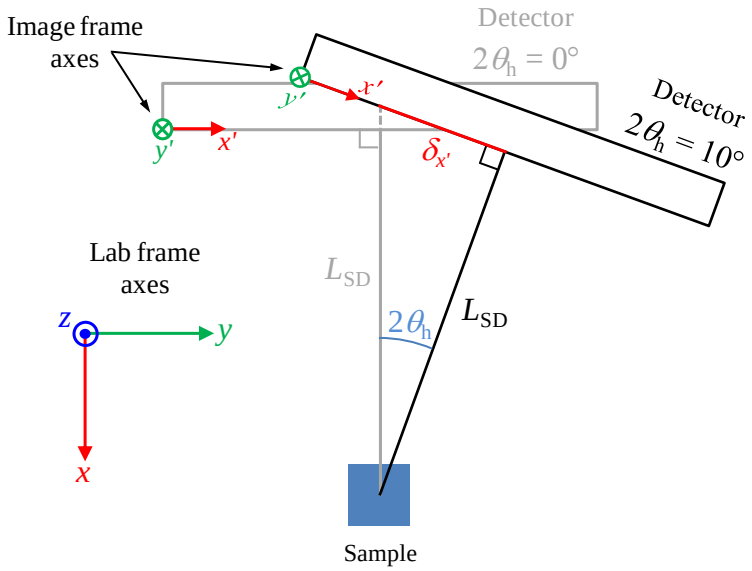

Fig. S1 Top-down view of the sample and detector geometry. The detector is rotated about the sample normal (*z*-axis) and an image taken. The detector angle $2\theta_h$ is known and the change in location of the direct beam δ_x is noted.

The change in the location of the direct beam on the image is noted. In the case of rotation about the lab frame *z*-axis by angle $2\theta_h$ the change in the *x*-location of the direct beam, $\delta_{x'}$, in the image frame is recorded. In the case of rotation about the lab frame *y*-axis by angle $2\theta_v$ the change in the *y*-location of the direct beam, $\delta_{y'}$, in the image frame is recorded. Using the known pixel size (in this case 77.28 μm × 77.28 μm), the sample-detector distance can be calculated as:[1]

$$L_{SD}(\text{mm}) = \frac{\delta_{x'} \times 0.07728}{\tan 2\theta_h} \tag{S1}$$

In the case of vertical detector rotation, $\delta_{x'}$ is replaced by $\delta_{y'}$ (the change in the direct beam location in the *y*-direction of the image frame) and $2\theta_h$ by $2\theta_v$ (the vertical detector rotation angle).

S1.2 Determination of scattering angles

The scattering angles for each pixel in the image are determined using trigonometric relationships between the sample-detector distance, L_{SD}, and the known pixel size. For simplicity, the sample-detector distance is converted to pixel units, *i.e.* L_{SD} (pixels) = L_{SD} (mm) / pixel size (mm). For the case of a detector oriented perpendicular to the incident beam the important relative pixel location that defines a right-angle is the direct beam location (x'_{dir}, y'_{dir}). In the case of a detector rotated about the *y*-axis, *i.e.* $2\theta_v \neq 0°$ (or about the *z*-axis, $2\theta_h \neq 0°$), the pixel location that defines a right-angle is the point of normal incidence (x'_N, y'_N); in other words, where direct beam would strike the detector if all detector angles were 0°. Only when the detector is oriented perpendicular to the incident beam does (x'_{dir}, y'_{dir}) = (x'_N, y'_N). A graphical representation of this geometric construction is shown in Fig. S2.

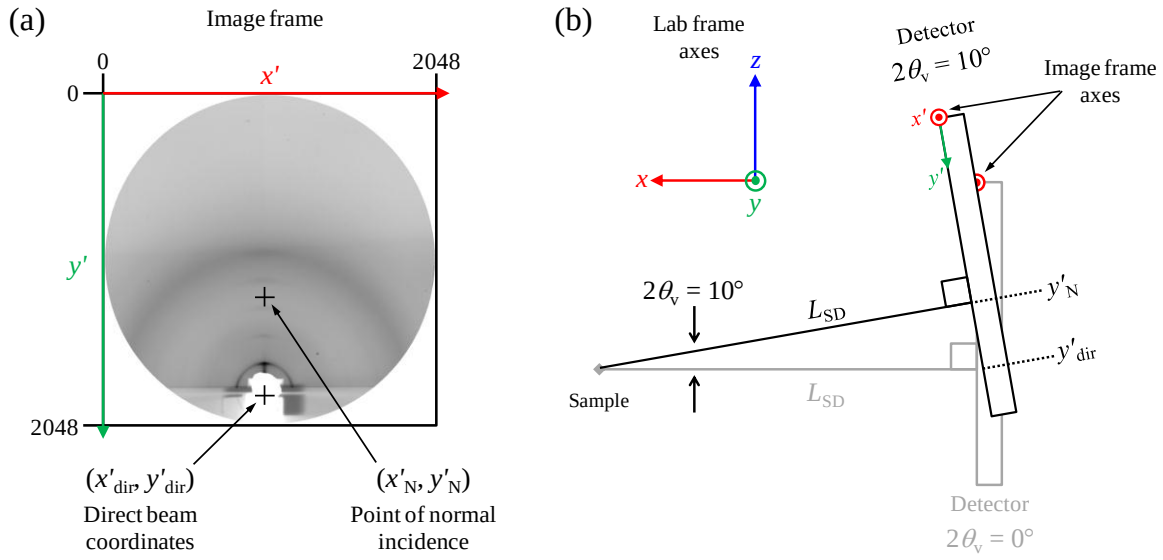

Fig. S2 (a) Image frame coordinate system (for detector tilted $2\theta_v = 10°$ about the y-axis) showing the positions of the direct beam and the point of normal incidence and (b) side view of a tilted detector.

When the detector is perpendicular to incident beam, *i.e.* $2\theta_v = 2\theta_h = 0°$, the out-of-plane ($\alpha_{f0}$) and in-plane ($2\theta_{f0}$) scattering angles in the lab frame for pixels of image coordinates (x'_{pix}, y'_{pix}) are calculated as follows:[1]

$$\alpha_{f0} = \text{atan}\left(\frac{y'_{pix} - y'_{dir}}{\sqrt{\left(x'_{pix} - x'_{dir}\right)^2 + {L_{SD}}^2}}\right) \tag{S2}$$

$$2\theta_{f0} = \text{atan}\left(\frac{x'_{pix} - x'_{dir}}{L_{SD}}\right) \tag{S3}$$

where x'_{dir} and y'_{dir} correspond to the coordinates of the direct beam in the image frame. However, when the detector is tilted, a correction term must be applied in order to correct for the resulting distortion. Here, the point of normal incidence (x'_N, y'_N) is used in place of the direct beam location, which is equivalent to the position of the direct beam when the detector is perpendicular to the incident radiation (*cf.* Fig. S2). The scattering angles are then calculated as follows:

$$\alpha_{f0} = \text{atan}\left(\frac{y'_{pix} - y'_N}{\sqrt{\left(x'_{pix} - x'_N\right)^2 + {L_{SD}}^2}}\right) + \tan\left(\frac{\tan 2\theta_v \times L_{SD}}{\sqrt{\left(x'_{pix} - x'_N\right)^2 + {L_{SD}}^2}}\right) \tag{S4}$$

$$2\theta_{f0} = \text{atan}\left(\frac{\left(x'_{pix} - x'_N\right) \times \cos 2\theta_v}{L_{SD}}\right) + 2\theta_h \tag{S5}$$

The additional terms are needed to account for distortion arising from the rotated detector. When the incident angle is non-zero, the in-plane scattering angle ($2\theta_f$) is constant (Equation S6), whether viewed from the surface frame or the lab frame; and the out-of-plane scattering angle (α_f) must be converted from the lab frame to the surface frame (Equation S7):

$$2\theta_{\mathrm{f}} = 2\theta_{\mathrm{f0}} \tag{S6}$$

$$\alpha_f = \alpha_{\mathrm{f0}} - \alpha_{\mathrm{i}} \cos(2\theta_{\mathrm{f}}) \tag{S7}$$

S1.3 Determination of reciprocal space coordinates

When the scattering angles are known, the wavevector transfer Q components (in-plane, Q_{xy}, and out-of-plane, Q_z) can be determined as follows:[1]

$$Q_z = k(\sin(\alpha_{\mathrm{f}}) + \sin(\alpha_{\mathrm{i}})) \tag{S8}$$

$$Q_x = k(\cos(\alpha_{\mathrm{f}}) \cos(2\theta_{\mathrm{f}}) - \cos(\alpha_{\mathrm{i}})) \tag{S9}$$

$$Q_y = k(\cos(\alpha_{\mathrm{f}}) \sin(2\theta_{\mathrm{f}})) \tag{S10}$$

$$Q_{xy} = \sqrt{{Q_x}^2 + {Q_y}^2} = k\sqrt{\cos^2(\alpha_{\mathrm{i}}) - 2\cos(\alpha_{\mathrm{i}})\cos(2\theta_{\mathrm{f}})\cos(\alpha_{\mathrm{f}}) + \cos^2(\alpha_{\mathrm{f}})} \tag{S11}$$

As a consequence of the planar detector intersecting the Ewald sphere of diffraction, certain data are not collected under the grazing-incidence geometry. The Q_z range of this limiting region, Q_{limit}, of observable scattering at a particular incident angle α_i can be estimated as:[1]

$$Q_{\mathrm{limit}} = \sqrt{2kQ_{xy} - {Q_{xy}}^2} \tag{S12}$$

A plot of the unobservable Bragg region (in red) using λ = 1.24 Å is shown in Fig. S3. Note, that the limiting region also has a dependence on the incident angle α_i, which is not accounted for in Equation (S12). The centre of this "splitting" follows the reflected beam, which is usually blocked by the beam stop.

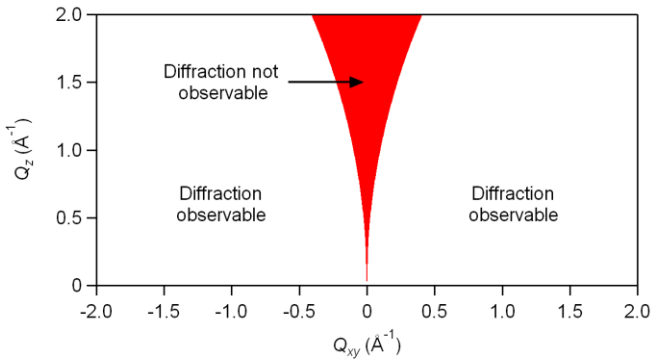

Fig. S3 The observable range of Bragg scattering calculated with a wavelength λ = 1.24 Å^{-1} for an incident angle α_i = 0. The portion of the reciprocal space map that is not observable is shown in red.

S1.4 Programmatic implementation of reciprocal space transformation

Diffraction data are typically recorded in relatively large files. For this experiment the images are 16-bit unsigned integer arrays with 2048 × 2048 pixels, which correspond to approximately 8 Mb per image. As a result, transforming a large number of images can be computationally expensive. Calculating the Q_{xy} and Q_z coordinates for each pixel followed by interpolation back to a 2D image is far too slow a process. As such images are transformed using the following algorithm:

1. The limit of observable data in *Q*-space is determined by calculating the *Q*-values for the four corner pixels of the *input* image.
2. A new (empty) *output* image matrix is generated spanning the range determined in Step 1. N.B. that the step size per pixel must be the same in the *x* and *y* directions.
3. A routine loops over every pixel in the *output* image and calculates backwards from the *Q*-values to the pixel coordinates containing the intensity information in the *input* image.
4. The calculated pixel coordinates for the *input* image are rarely integer values, therefore to determine the correct intensity value to fill the pixel in the *output* image a 2D interpolation is used each time (this improves the accuracy of intensity data and does not affect the processing time significantly).

S1.5 Refraction correction

X-rays crossing an interface – either entering or exiting – are subjected to refraction effects, particularly at low angles. This phenomenon affects only the vertical component of the wavevectors (perpendicular to the interface), k_{zi} and k_{zf}, the incident and reflected wavevectors respectively. As a consequence, the incident angle within the film is smaller than the incident angle at the helium-film interface (*cf.* Fig. S4) and the calculated wavevector transfer component perpendicular to the interface, Q_z, is slightly greater than the true Q_z inside the film. For accurate determination of Q_z and the corresponding *d*-spacing of Bragg reflections, these effects must be accounted for.

The refractive index of a medium to X-rays is given by:[2]

$$n = 1 - \delta + i\beta \tag{S13}$$

where the scattering and absorption properties of the medium are given by δ and β, respectively. The δ coefficient is related to the electron density of the medium, ρ, and the classical electron radius, r_0 (2.818 × 10^{-15} m), through Equation (S14). The β coefficient is determined by the absorption coefficient, μ, through Equation (S15).

$$\delta = \frac{2\pi\rho r_0}{k^2} \tag{S14}$$

$$\beta = \frac{2\mu}{k} \tag{S15}$$

where k is the wavenumber. The refractive index, n, is therefore slightly smaller than unity. As a result, a wave of X-rays incident on a medium at incident angle α_i is refracted as it travels through the film as shown in Fig. S4.

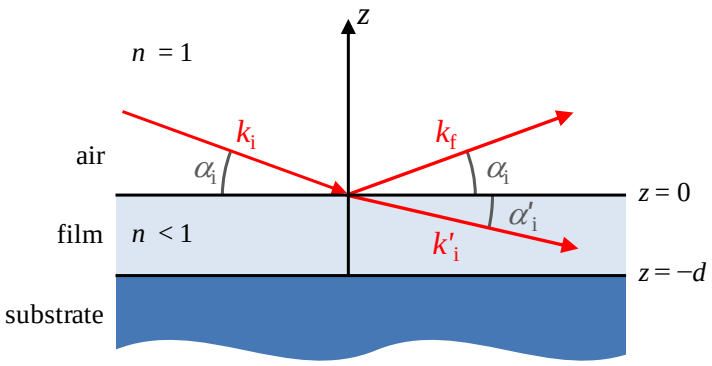

Fig. S4 X-rays incident on a film at angle α_i are refracted perpendicular to the interface resulting in an effective incident angle within the film, α'_i, slightly smaller than α_i, the vacuum incident angle.

The incident angle within the film, α'_i, is dependent on the vacuum incident angle and the refractive index, n. Using a Taylor expansion of Snell's law, α'_i can be related to the δ and β coefficients or the critical angle, α_c, through the following equations:

$$\begin{aligned} \alpha^2 &= \alpha'^2 + 2\delta - 2i\beta \\ &= \alpha'^2 + \alpha_c^2 - 2i\beta \end{aligned} \tag{S16}$$

The component of the wavevector transfer parallel to the interface, Q_{xy}, is unaffected by refraction effects. The perpendicular component of the wavevector transfer is given by:

$$Q_z = k(\sin\alpha_i + \sin\alpha_f) \tag{S17}$$

where α_i and α_f are the incident and reflected angles respectively. This equation however, does not take into account the refraction within the film. Both the incident (k_{zi}) and reflected (k_{zf}) wavevectors must be corrected and are derived from the relationship between incident and transmitted angles derived from Snell's law as shown in Equation S16:[1, 3]

$$k'_{zi} = \sqrt{k_{zi}^2 - k_c^2} = k\left(\sqrt{\sin^2\alpha_i - \sin^2\alpha_c}\right) \tag{S18}$$

$$k'_{zf} = \sqrt{k_{zf}^2 - k_c^2} = k\left(\sqrt{\sin^2\alpha_f - \sin^2\alpha_c}\right) \tag{S19}$$

where k_c is the critical wavevector given by the critical angle, α_c:

$$k_c = k(\sin\alpha_c) \tag{S20}$$

This equation can be expressed in full as:

$$Q'_z = k'_{zf} + |k'_{zi}| \tag{S21}$$

$$= k\left((\sin^2\alpha_i - \sin^2\alpha_c)^{\frac{1}{2}} + (\sin^2\alpha_f - \sin^2\alpha_c)^{\frac{1}{2}}\right) \tag{S22}$$

Refraction corrected Q'_z values for exit angle smaller than α_c cannot be evaluated as the corrected exit wavevector, k'_{zf}, contains a square root term of a negative value ($\sin^2\alpha_f - \sin^2\alpha_c$, where $\alpha_f < \alpha_c$). For this reason it is simpler not to apply the refraction correction during the complete image transformation but instead during line profile extraction. Solving Equation S17 for α_f gives:

$$\alpha_f = \text{asin}\left(\frac{Q_z}{k} - \sin\alpha_i\right) \tag{S23}$$

By substituting the result of Equation S23 into the expression for the refraction corrected Q'_z term given by Equation 22 the corrected Q_z value can be determined from a measured (uncorrected) Q_z value from the images as follows:

$$Q'_z = k\left((\sin^2\alpha_i - \sin^2\alpha_c)^{\frac{1}{2}} + \left(\sin^2\left(\text{asin}\left(\frac{Q_z}{k} - \sin\alpha_i\right)\right) - \sin^2\alpha_c\right)^{\frac{1}{2}}\right) \tag{S24}$$

The difference in the corrected Q'_z term is therefore dependent both on the incident angle and the magnitude of the uncorrected Q_z term. To illustrate the importance of this correction, the difference between corrected and uncorrected Q_z values (ΔQ_z) is plotted as a function of the uncorrected Q_z term for three incident angles in Fig. S5.

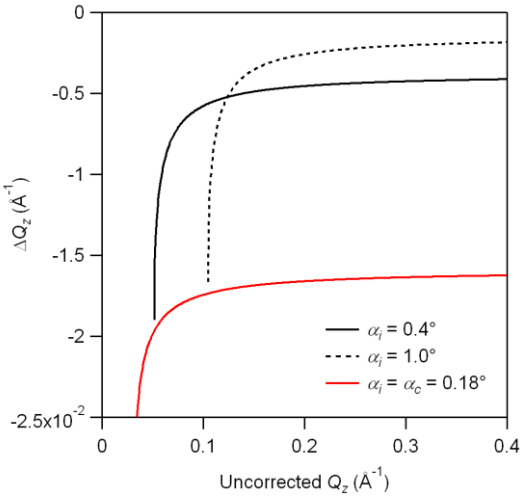

Fig. S5 Magnitude of the Q_z correction term (ΔQ_z) as a function of uncorrected Q_z value for three different incident angles. The correction term is greatest when the incident and exit wave vectors are of a similar magnitude (low Q_z) and at higher Q_z the correction term depends mostly on the incident angle.

The corrected Q'_z term can then be used to determine the true out-of-plane *d*-spacing:

$$d' = \frac{2\pi}{Q'_z} \tag{S25}$$

For reflections containing both Q'_z and Q_{xy} terms the absolute wavevector transfer is given by:

$$Q = \sqrt{Q'^2_z + Q^2_{xy}} \tag{S26}$$

And the corresponding *d*-spacing by:

$$d' = \frac{2\pi}{Q} \tag{S27}$$

S1.6 Refractive index values

The δ and β coefficients of the refractive index are required for calculation of the refraction effects and thus are necessary for accurate determination of reciprocal space coordinates. These values were determined using the Centre for X-ray Optics online resource.[4] The density of each material was not known and so was estimated by the calculation software. For each sample the density was estimated to be 2.2 g/cm^3. The critical angle is defined as $\alpha_c = (2\delta)^{1/2}$.

Table S2 Calculated δ, β and α_c values for each of the samples studied in this report.

Compound	Formula	δ	β	Critical angle (°)
TANI(EB)	$C_{30}H_{24}N_4$	4.82E-06	4.93E-09	0.178
TANI(BEHP)$_{0.5}$	$C_{62}H_{94}N_4O_8P_2$	4.96E-06	1.01E-08	0.180
OANI(EB)	$C_{54}H_{42}N_8$	4.81E-06	4.98E-09	0.178
OANI(BEHP)$_{0.5}$	$C_{118}H_{182}N_8O_{16}P_4$	4.96E-06	1.03E-08	0.181
Silicon	Si	4.89E-06	7.39E-08	0.179

S1.7 Calculation of penetration depth

The penetration depth of the incident beam, *i.e.* the depth through a material at which the intensity has decayed to 1/e, Λ_i, is given by:[5]

$$\Lambda_i^{-1} = \sqrt{2}k\left(\sqrt{(\alpha_i^2 - \alpha_c^2)^2 + 4\beta^2} + \alpha_c^2 - \alpha_i^2\right)^{1/2} \tag{S28}$$

The penetration depth as a function of incident angle for a BEHP-doped oligo(aniline) film (with typical parameters: $\delta = 5\times10^{-6}$ and $\beta = 1\times10^{-8}$) at wavelength λ = 1.24 Å is given in Fig. S6. The incident angle used in most of our GIXS experiments was selected to be 0.4° (*cf.* dashed line in Fig. S6) at which the penetration depth into a typical oligo(aniline) film is approximately 6000 nm (*cf.* red curve in Fig. S6). This ensures complete illumination of the films (~350 nm thick) whilst minimizing the scattering from the silicon substrate (Λ_i for silicon ~800 nm at α_i = 0.4°; *cf.* blue curve in Fig. S6).

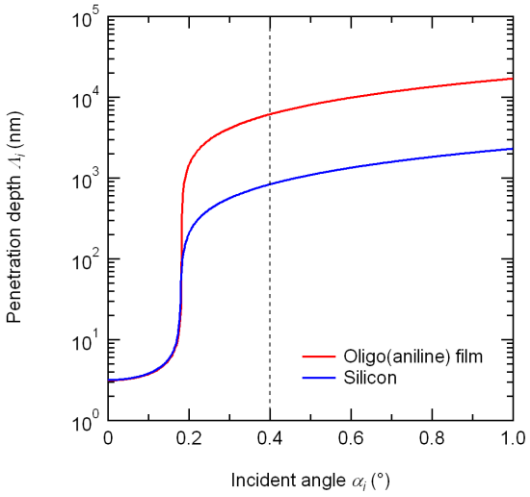

Fig. S6 Calculated penetration depth as a function of incident angle for a typical oligo(aniline) film (red curve) and silicon (blue curve). The dashed line indicates the typical incident angle used for our GIXS experiments (α_i =0.4°).

S2 Additional Results

S2.1 TANI

S2.1.1 TANI(EB) line profile

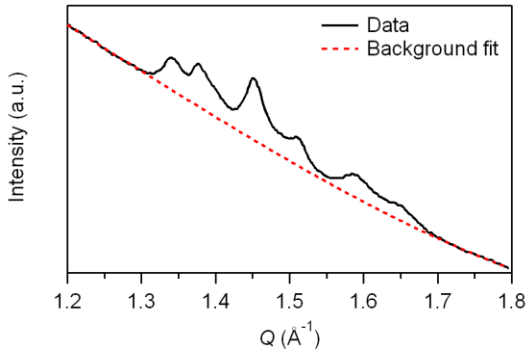

Fig. S7 Raw line profile data for TANI(EB) film and the fitted cubic background function which was subtracted from the data for clarity as shown in Fig. 3b in the main text.

S2.1.2 Indexation of the TANI(BEHP)$_{0.5}$ diffraction pattern

This is relevant to Section 3.3 in the main text, "Thin film lattice structure of oligomer-surfactant complexes", and the 2D scattering image we refer to in the following Section is shown in Fig. 5(a) of the main text and also shown in Fig. S9.

The hexagonal lattice is first assumed based on the relationship between certain families of reflections. At 60° (about the origin of reciprocal space) relative to the first and second order out-of-plane lamellar reflections are two reflections with the same magnitude wavevector transfer, *Q*. This can be seen clearly in the Azimuthal integration about the 2nd order lamellar reflection shown in Fig. S8. This observation suggests hexagonal symmetry.

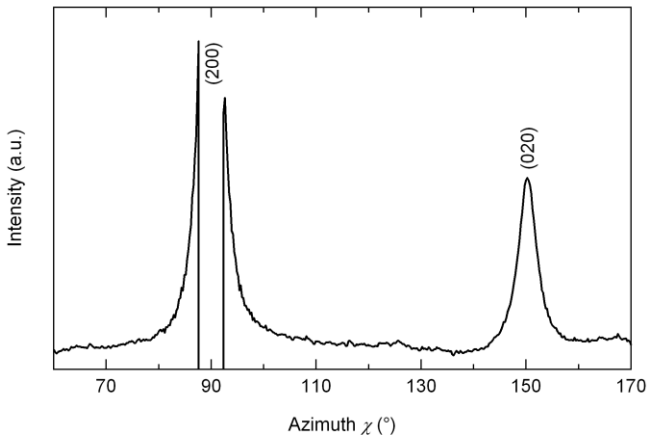

Fig. S8 Azimuthal integration around the ring defining the second order reflections. At χ = 90°, the (200) reflection is observed. Note the peak is missing the middle portion of data as a result of the splitting caused by the grazing-incidence geometry. At $\Delta\chi$ = 60° relative to this reflection (χ = 150°) occurs the (020) reflection.

To determine the unit cell lattice parameters for the TANI(BEHP)$_{0.5}$ sample, first the experimentally observed reflections are fitted with 2D Gaussian functions to extract the exact reciprocal space coordinates (*cf.* Fig. S9a).

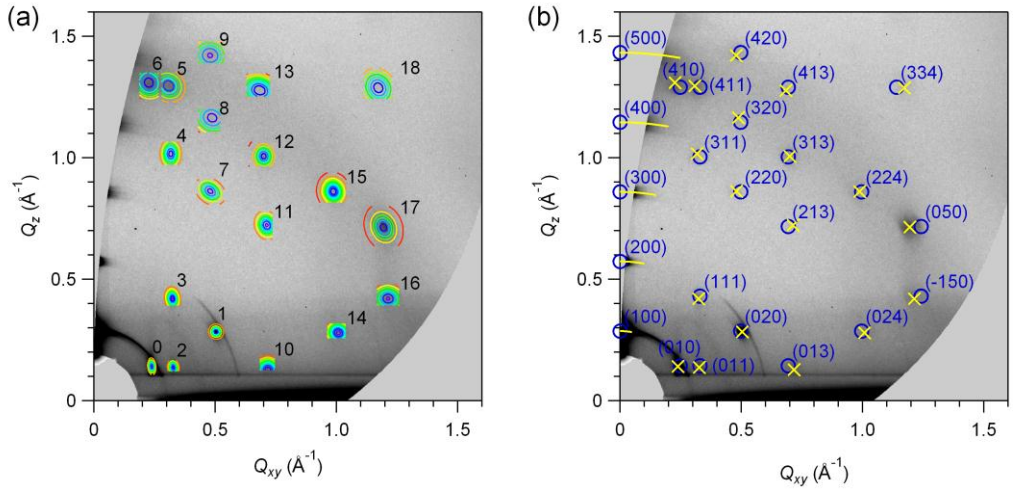

Fig. S9 (a) 2D Gaussian fits to diffraction peaks are superimposed as contour plots on the raw data; (b) reflection maxima extracted from 2D Gaussian fits (yellow crosses) and calculated reflections based on the model unit cell (blue circles). Miller indices for the calculated reflections have been assigned. The yellow arcs extending anticlockwise from Q_{xy} = 0 represent the out-of-plane peak positions, the diffuse off-specular scattering arising from these peaks are observed.

Using the assumed 2D hexagonal lattice (a = b = 2.54 nm and γ = 120°) as a starting point the diffraction pattern is indexed following the method proposed by Smilgies and Balsini.[6] Firstly, the reciprocal lattice is described by the reciprocal lattice vectors:

$$\mathbf{a}^* = \begin{bmatrix} a^* \\ 0 \\ 0 \end{bmatrix} \qquad \mathbf{b}^* = \begin{bmatrix} b^*\cos(\gamma^*) \\ b^*\sin(\gamma^*) \\ 0 \end{bmatrix} \qquad \mathbf{c}^* = \begin{bmatrix} c^*\cos(\beta^*) \\ -c^*\sin(\beta^*)\cos(\alpha) \\ 2\pi/c \end{bmatrix} \tag{S29}$$

where α and c are the direct lattice parameters and a*, b*, c*, β* and γ* are the reciprocal lattice parameters. The next step is to orient the reciprocal lattice to relative to the surface plane using a known oriented reflection. It is assumed that the *ab*-

plane lies parallel to the surface normal, with the *b*-axis parallel to the substrate so that the out-of-plane reflections correspond to the (*h*00) family. Thus the (100) is the orientated reflection (*i.e.* that which is parallel to the surface normal). This oriented reflection satisfies the following condition:

$$\mathbf{g}_{hkl} = h\mathbf{a}^* + k\mathbf{b}^* + l\mathbf{c}^* \tag{S30}$$

From this oriented reflection, the rotation angles defining the oriented crystal are calculated. Note that the crystal only needs orienting in two dimensions. This is because the crystal has a preferential orientation relative to the substrate plane; however, within the plane of the film the crystallites display random orientation, similar to the so-called fibre texture. The orientation of the crystallites is described by the following two angles,

$$\varphi = \text{atan2}[(\mathbf{g}_{hkl})_2, (\mathbf{g}_{hkl})_1] \tag{S31}$$

$$\chi = \text{acos}[(\mathbf{g}_{hkl})_3/|\mathbf{g}_{hkl}|] \tag{S32}$$

where $(\mathbf{g}_{hkl})_i$ is the *i*th Cartesian coordinate of the oriented reflection vector and $|\mathbf{g}_{hkl}|$ is the absolute value (*i.e.* modulus). Note that in the paper by Smilgies and Blasini, the $(\mathbf{g}_{hkl})_2$ and $(\mathbf{g}_{hkl})_1$ are switched in the atan2 term of Equation (S31). This gives a different mathematical and we have found that it is necessary to use the expression in the format of Equation (S31). Using these rotation angles, a rotation matrix can be constructed:

$$\boldsymbol{R} = \begin{bmatrix} \cos(\chi) & 0 & \sin(\chi) \\ 0 & 1 & 0 \\ -\sin(\chi) & 0 & \cos(\chi) \end{bmatrix} \begin{bmatrix} \cos(\varphi) & \sin(\varphi) & 0 \\ -\sin(\varphi) & \cos(\varphi) & 0 \\ 0 & 0 & 1 \end{bmatrix} \tag{S33}$$

This rotation matrix is in a slightly different form to that in the Smilgies and Blasini paper. To check the correctness of the expression, we note that the determinant of a rotation matrix (Equation S33) must equal 1, as in our case. Multiplication of the reciprocal lattice vectors by the rotation matrix yields the oriented reciprocal lattice vectors relative to the surface frame:

$$\mathbf{a}_{\mathrm{R}}^* = \boldsymbol{R} \cdot \mathbf{a}^* \qquad \mathbf{b}_{\mathrm{R}}^* = \boldsymbol{R} \cdot \mathbf{b}^* \qquad \mathbf{c}_{\mathrm{R}}^* = \boldsymbol{R} \cdot \mathbf{c}^* \tag{S34}$$

The wavevector transfer, **q**, for a reflection of Miller indices (*hkl*) is calculated as follows:

$$\mathbf{q} = h\mathbf{a}_{\mathrm{R}}^* + k\mathbf{b}_{\mathrm{R}}^* + l\mathbf{c}_{\mathrm{R}}^* \tag{S35}$$

The **q** vector can be expressed in terms of the parallel (Q_{xy}) and perpendicular (Q_z) components through the following relationships:

$$Q_{xy} = (\mathbf{q}_1^2 + \mathbf{q}_2^2)^{1/2} \tag{S36}$$

$$Q_z = \mathbf{q}_3 \tag{S37}$$

Using these relationships, the lattice parameters can be refined to match the calculated reflections with the experimentally observed reflections. A program has been written to perform this analysis in IgorPro (WaveMetrics®). The results of this

data fitting, using the lattice parameters $a = b = 2.53$ nm, $c = 2.91$ nm and $\gamma = 120°$, to the TANI(BEHP)$_{0.5}$ GIXS pattern are shown in Fig. S9b. The reciprocal space coordinates for the experimentally observed reflections and the calculated reflections of Miller indices (*hkl*) are shown in Table S3.

Table S3 Comparison of the reciprocal space coordinates for the calculated lattice and the experimental data. The error values for the experimental data are the σ values returned from the 2D Gaussian fit to each ref`lection. The difference values are calculated as (Q(calculated) − Q(experimental)). Note that the (h00) reflections have not been included as their exact location cannot be extracted from the GIXS patterns.

Index	**Experimental** (Å^{-1})				**Calculated** (Å^{-1})		**Difference** (Å^{-1})	
(*hkl*)	Q_{xy}	Error	Q_z	Error	Q_{xy}	Q_z	ΔQ_{xy}	ΔQ_z
(010)	0.239	0.0001	0.142	0.0001	0.248	0.143	0.010	0.002
(020)	0.504	0.0001	0.285	0.0001	0.497	0.287	-0.007	0.002
(011)	0.327	0.0002	0.137	0.0004	0.328	0.143	0.000	0.006
(111)	0.324	0.0001	0.420	0.0002	0.328	0.430	0.004	0.010
(311)	0.317	0.0004	1.017	0.0005	0.328	1.004	0.011	-0.013
(411)	0.308	0.0002	1.296	0.0002	0.328	1.290	0.019	-0.006
(410)	0.226	0.0002	1.310	0.0002	0.248	1.290	0.022	-0.019
(220)	0.480	0.0005	0.863	0.0004	0.497	0.860	0.017	-0.002
(320)	0.488	0.0011	1.165	0.0009	0.497	1.147	0.009	-0.018
(420)	0.479	0.0003	1.421	0.0004	0.497	1.434	0.018	0.012
(013)	0.718	0.0005	0.128	0.0013	0.688	0.143	-0.030	0.016
(213)	0.713	0.0009	0.723	0.0008	0.688	0.717	-0.025	-0.006
(313)	0.700	0.0002	1.007	0.0002	0.688	1.004	-0.013	-0.003
(413)	0.684	0.0013	1.278	0.0014	0.688	1.290	0.004	0.013
(024)	1.008	0.0005	0.280	0.0005	0.989	0.287	-0.019	0.007
(224)	0.987	0.0003	0.862	0.0003	0.989	0.860	0.001	-0.002
(-150)	1.213	0.0003	0.421	0.0003	1.242	0.430	0.028	0.010
(050)	1.194	0.0001	0.714	0.0001	1.242	0.717	0.047	0.003
(334)	1.173	0.0005	1.288	0.0005	1.134	1.290	-0.039	0.002

S2.1.3 TANI(BEHP)$_{0.5}$ thermal annealing

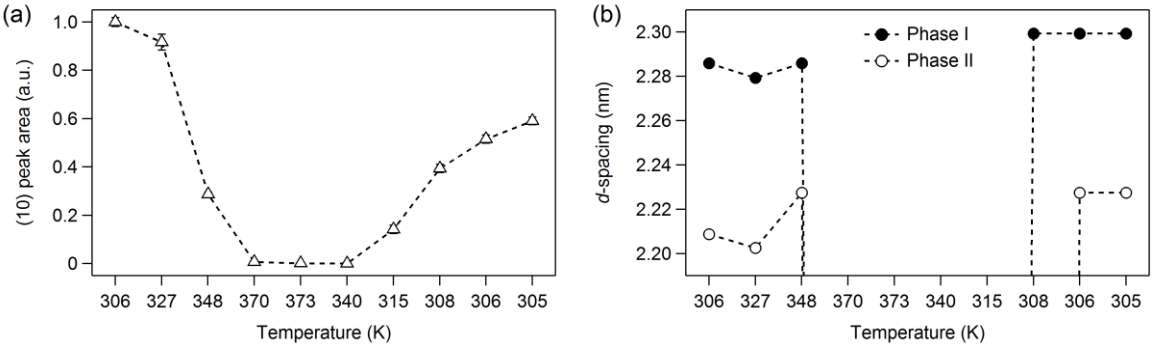

Fig. S10 (a) Intensity of the (10) reflection as a function of sample temperature. After annealing the intensity of the first order reflection is <60% of the pre-anneal value. This is either due to kinetic trapping of some molecules in a disordered state as a result of rapid cooling or beam damage of the sample after sustained exposure to X-ray radiation. (b) *d*-spacing of the Phase I and Phase II lamellae during thermal

annealing as determined from the (20) reflection. There are very slight changes to the lamellar distances in both Phase I and Phase II and the order-disorder transition is evident from absence of (20) reflections between 348 K and 308 K.

S2.2 OANI

S2.2.1 OANI(BEHP)$_{0.5}$ azimuthal integration

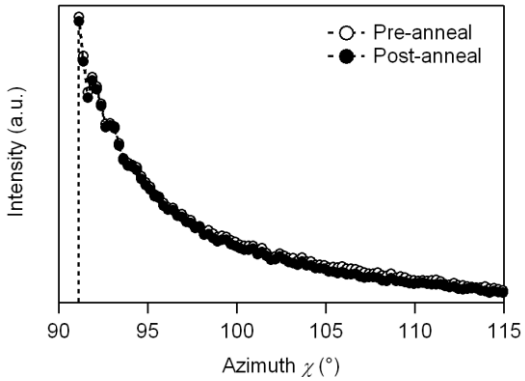

Fig. S11 Azimuthal integration around the (10) reflection for the OANI(BEHP)$_{0.5}$ film before (open circles) and after (closed circles) thermal annealing. There is little difference between the two traces indicating that there is no change in the degree of orientation of OANI(BEHP)$_{0.5}$ crystallites relative to the substrate after thermal annealing.

S3 References

1. D. M. Smilgies, *WAXS / GIWAXS @ D1: Conversions*, http://staff.chess.cornell.edu/~smilgies/D-lineNotes /GISAXS-at-D-line/GIWAXS@D1_Conversions.html. Retrieved: May 17, 2013
2. J. Als-Nielsen and D. McMorrow, *Elements of Modern X-Ray Physics*, Wiley, Chichester, England, 2001.
3. P. Busch, M. Rauscher, D. M. Smilgies, D. Posselt and C. M. Papadakis, *J. Appl. Crystallogr.*, 2006, **39**, 433-442.
4. E. Gullikson, The Centre for X-ray Optics, 2010, *X-Ray Interactions With Matter*, http://henke.lbl.gov /optical_constants/ Retrieved: May 17, 2013; and B.L. Henke, E.M. Gullikson, and J.C. Davis, *Atomic Data and Nuclear Data Tables*, 1993, **54**, 2, 181-342.
5. R. Feidenhans'l, *Surf. Sci. Rep.*, 1989, **10**, 105-188.
6. D. M. Smilgies and D. R. Blasini, *J. Appl. Crystallogr.*, 2007, **40**, 716-718.